



Where should the thermal image sensor of a smart A/C look?-Occupant thermal sensation model based on thermal imaging data

Junmeng Lyu ^a, Heng Du ^a, Zisheng Zhao ^b, Yongxiang Shi ^a, Bo Wang ^b, Zhiwei Lian ^{a,*}

^a School of Design, Shanghai Jiao Tong University, Shanghai, 200240, China

^b Guangdong Midea Air-Conditioning Equipment Co., Ltd, Guangdong, 528311, China



ARTICLE INFO

Keywords:

Thermal sensation model
Two-stage model
Thermal image sensor
Smart air conditioner

ABSTRACT

Applying thermal imaging sensor to air conditioner for monitoring human thermal sensation and achieving dynamic settings may satisfy occupants' thermal needs while saving energy. The existing studies are mostly based on single-view imaging to build the model and ignore the possible differences in body surface temperature on thermal sensation response by gender, etc., which may have many limitations. Subject experiments were conducted in an artificial climate chamber to obtain subjective questionnaires and thermal images of the exposed frontal face, lateral face, top of the head, forearm, and hand dorsum of 27 subjects in this study. By applying machine learning classification algorithms and global optimal regression algorithms, the temperature collection zones that can accurately reflect the thermal sensation of both genders in each view were analyzed, and a two-stage thermal sensation assessment model applicable to multiple views was developed. Of the various imaging views, the frontal view of the face is the best, followed by the lateral view of the face, the top view of the head, and the forearm/hand dorsum view. For male and female, the mean absolute errors of the thermal sensation assessment model established were 0.41–0.49 and 0.50–0.53 thermal sensation units. In addition, gender differences were found in the response of head surface temperatures to thermal sensation. The results obtained can provide a reference for the application of thermal image sensor to smart air conditioners.

1. Introduction

HVAC (Heating, ventilation, and air conditioning) systems are responsible for over 30% of global energy consumption-with the aim of meeting the thermal preferences of occupants in the indoor environment [1]. Numerous occupants tend to set their air conditioner (A/C) at the default values recommended by the standards [2,3], which can result in inefficient energy usage and may not satisfy everyone's demands due to individual differences [4,5]. Therefore, it is imperative to explore ways to optimize HVAC system operation for the provision of a more energy-efficient and satisfactory thermal environment.

Thermal sensation is a critical factor that significantly impacts an individual's comfort within an indoor environment [6]. The PMV model proposed by Fanger is a landmark model of thermal sensation [7]. This model quantifies human thermal sensation as a range from -3 (cold) to +3 (hot). However, the application of the PMV model in controlling smart A/C is restricted due to the lack of real-time availability of non-environment parameter inputs and the disregard for individual thermal sensation difference, rendering the implementation ineffective

[8,9]. The advancement of thermal comfort theory and sensor technology has significantly contributed to the development of smart A/C. The present researches on smart A/C auto-control frameworks can be broadly categorized into three categories. The first is real-time monitoring of user actions and clothing using image recognition algorithms to achieve thermal sensation assessment or dynamic input of metabolic rate and clothing level of PMV model [10,11]. The second involves using machine learning algorithms to establish user behavior models based on large amounts of historical A/C usage data to drive A/C setpoint adjustment [12]. The third category focuses on building models to correlate physiological parameters with thermal sensation. This is accomplished by combining physiological parameter monitoring devices with A/C, using physiological data to evaluate thermal sensation and drive automatic setpoint adjustment [13,14].

The human body perceives temperature through cold- and heat-sensitive nerve endings under the skin, which transmit signals to the hypothalamus via the sympathetic nervous system [15]. Hot and cold sensations in humans control the contraction and dilation of blood vessels flowing through the body surface, resulting in changes in skin temperature that correlate with thermal sensation. Factors such as fat

* Corresponding author.

E-mail address: zwlian@sjtu.edu.cn (Z. Lian).

Abbreviations	
A/C	Air conditioner
HVAC	Heating, ventilation, and air conditioning
MAE	Mean absolute error
T _{Air}	Indoor air temperature, °C
T _{Arm}	Forearm surface temperature, °C
T _{F-F}	Forehead surface temperature from the frontal view, °C
T _{F-C}	Cheek surface temperature from the frontal view, °C
T _{F-N}	Nose surface temperature from the frontal view, °C
T _{F-M}	Surface temperature around the mouth from the frontal view, °C
T _{F-Min}	The minimum surface temperature of four zones captured from frontal view, °C
T _{F-Max}	The maximum surface temperature of four zones captured from frontal view, °C
T _{F-Mean}	The mean surface temperature of four zones captured from frontal view, °C
T _{F-ED}	The range of the temperature differences between zones captured from frontal view, °C
T _{F-SD}	The standard deviation of the temperature differences between zones captured from frontal view, °C
T _{Hand}	Hand dorsum surface temperature, °C
T _{Overhead}	Overhead surface temperature, °C
T _{S-C}	Cheek surface temperature from the lateral view, °C
T _{S-F}	Forehead surface temperature from the lateral view, °C
T _{S-E}	Ear helix surface temperature from the lateral view, °C
T _{S-N}	Nose surface temperature from the lateral view, °C
T _{S-Min}	The minimum surface temperature of four zones captured from lateral view, °C
T _{S-Max}	The maximum surface temperature of four zones captured from lateral view, °C
T _{S-Mean}	The mean surface temperature of four zones captured from lateral view, °C
T _{S-ED}	The range of the temperature differences between zones captured from lateral view, °C
T _{S-SD}	The standard deviation of the temperature differences between zones captured from lateral view, °C
V _{Air}	Indoor air velocity, m/s

thickness [16], metabolic rate, and hormone levels [17] play a role in regulating vascular flow on the human body surface, indicating that skin temperature contains certain population-specific information [18]. Existing studies have utilized physiological sensors to collect skin temperature and develop thermal sensation models based on these theoretical studies [19–21]. Xie et al. [22] summarized the skin temperature collection techniques involved in thermal comfort studies and categorized skin temperature measurement devices as invasive, semi-invasive, and non-invasive. Initially, thermocouples were used to measure skin temperature, which is an invasive device with high accuracy and fast response. As thermocouples became wireless and infrared ray technology matured, semi-invasive instruments were introduced for skin temperature measurements. However, both invasive and semi-invasive sensors have limitations in controlling HVAC set points. In everyday scenarios, it is impractical to necessitate the continuous attachment of a wired thermocouple to an individual's body surface. For semi-invasive sensors, researchers have proposed the integration of sensors with wearable devices (e.g., smartwatches, glasses) to facilitate temperature monitoring. However, this approach increases the weight of the wearable device and obliges users to buy and consistently wear the device to drive HVAC automatic control effectively [23].

The development of uncooled detectors has facilitated the widespread adoption of thermal imaging technology for civilian applications. In recent years, advancements in thermal imaging technology, coupled with increased production capacity, have led to improvements in the accuracy and resolution of thermal imaging sensors, while simultaneously reducing costs [24]. This non-invasive technology has garnered the attention of some scholars, who are increasingly utilizing it for thermal sensation studies [13,21,25–31]. The use of thermal imaging technology provides an uninterrupted and efficient way of monitoring the exposed skin temperature of occupants, thereby enabling accurate prediction of their thermal sensation. Li et al. [25] proposed a real-time thermal sensation prediction framework that uses thermal imaging. By integrating features collected from different facial zones, the framework predicted the thermal preferences of subjects with an accuracy of 85%. He et al. [27] built a thermographic temperature and thermal sensation model using a dataset obtained from an experiment with a 96% accuracy rate. Although the similarity of the temperature data and the over-sampling of data in the test set may have overestimated the model's performance, this research retains significant reference value. Cosma et al. [28] employed a fusion sensing system to extract skin and clothing temperatures of subjects to develop a thermal sensation model. The

relationships and characteristics of these studies are depicted in Fig. 1.

The research on the application of thermal imaging for thermal sensation assessment is currently undergoing rapid development. However, there remain several issues that require attention. One of the primary limitations is that the models proposed in established studies are applicable only for thermal imaging from a single perspective. In practical application, users are not required to maintain a fixed position relative to the thermal imaging sensor. This presents a challenge for the application of such models, as the imaging view can significantly influence their effectiveness. Li et al. [26] acknowledged this limitation in their study and suggested that it can be mitigated by deploying more sensors in the room. Nevertheless, the cost of smart A/C rises proportionally with the number of sensors. Additionally, some models require the input of surface temperatures of multiple body segments [28,30]. The abundance of temperature information input can hinder the practical application of the model due to the imbalance between the field of view, imaging distance, and imaging accuracy of thermal imaging sensors [29].

The head, forearm, and hand dorsum are often exposed to the surrounding environment for prolonged periods without any clothing coverage in summer, which makes it more susceptible to the influence of ambient temperature. Several subject experiments have revealed a correlation coefficient exceeding 0.6 between thermal sensation and skin temperature of the face, forearm, and hand dorsum, despite these surface area accounting for less than 20% of the total body surface area [29,32,33]. This exposure also facilitates the non-invasive collection of corresponding surface temperatures using thermal imaging sensors. The surface temperature of facial zones may exhibit varying response sensitivities to thermal sensation. Areas with greater blood flow (e.g. cheeks, nose) as well as thinner subcutaneous fat layer (e.g. ears) were often reported to vary more significantly with environmental temperatures than in other areas [32,34]. It may be more accurate to screen the zones that are most sensitive to thermal sensation and use their surface temperature to build model. In addition, some studies have investigated the differences in skin temperature sensitivity between males and females in air-conditioned environments, with most focusing on limb skin temperature [35,36]. These studies have consistently found that female limb skin is more sensitive than male skin in cold environments. However, it is important to note that there may be significant gender differences in head surface temperature due to differences in head fat and muscle thickness [37]. Therefore, possible gender differences in head surface temperature need to be further clarified. Given the potential

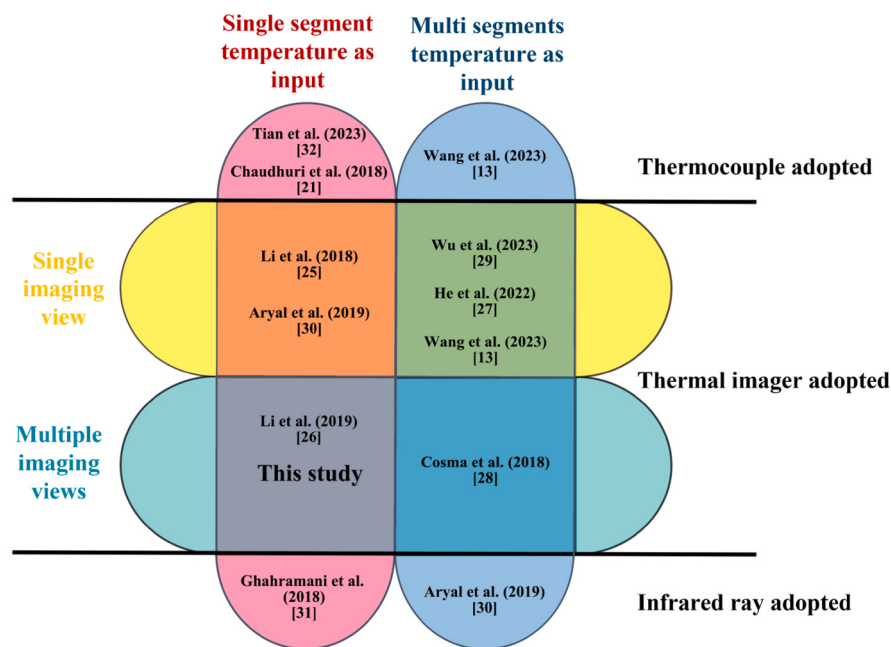


Fig. 1. Relationship between existing studies and this study.

presence of users of different genders in the utilization of smart A/C that incorporate thermal imaging sensors, it may be worthwhile to account for gender differences as a critical factor in the thermal sensation assessment model.

To address these limitations, a range of environments with varying indoor air temperatures and air velocities were established within an artificial climate chamber in this study. The thermal sensation of the subjects was evaluated using ASHRAE 7-point vote, while a thermal camera was utilized to capture thermal images of the subjects' frontal face, lateral face, top of the head, forearm, and hand dorsum surface (no clothing coverage). Temperature information from specific zones was then extracted, and combined with machine learning classification and regression algorithms to analyze surface temperature acquisition zones that accurately reflect thermal sensation in each imaging perspective for different genders. Ultimately, a thermal sensation assessment model was developed for both genders based on multiple thermal imaging views.

2. Methodology

2.1. Accuracy evaluation of the thermal camera

In this study, high performance thermal imaging camera (FLIR T-460; Teledyne FLIR, Wilsonville, Oregon, USA) was used to collect surface temperatures of head, forearm, and hand dorsum from the subjects. The description of this thermal imaging camera is listed in Table 1. The thermal camera employed in this study boasts a resolution of 320×240 pixels and features an integrated 3.1-megapixel visible digital camera. This enables the clear delineation of distinct head

regions, resulting in the acquisition of more detailed information and improved accuracy of temperature readings. It was factory calibrated and equipped with an automatic flat field calibration feature to counteract reading drift effects [30]. The emissivity was set to 0.98 [27], and the reflective temperature was adjusted to match the indoor air temperature during the experiments. Thermal imaging cameras are subject to systematic errors that may arise from various factors such as sensor element efficiency and sensor temperature [38]. Therefore, prior to conducting the formal experiments, this study conducted a pre-experiment to compare the skin temperature measurements obtained through the Pyrobutton (Opulus, Philadelphia, Pennsylvania, USA) with those acquired using FLIR T-460. For skin temperature measurement, the Pyrobutton has proven to be a dependable instrument, as detailed in Table 1. The objective of this comparison was to establish the validity of FLIR T-460 for human skin temperature measurements. Details of the pre-experiment is provided in the Supplementary Material S1. The difference in readings between the FLIR T-460 and Pyrobutton for face temperature acquisition in indoor environments from 23°C to 30°C is less than 0.3°C . These findings align with those reported in the validation study conducted by Wu et al. [29]. Findings indicate that the thermal imaging camera FLIR T-460 utilized in this study is appropriate for collecting human skin temperature.

2.2. Data collection

To investigate the correlation between thermal sensation and body surface temperature as measured through thermal imaging, a series of subject experiments were conducted in an artificial climate chamber at Shanghai Jiao Tong University between August and September 2022 (summertime). The climate was hot and humid (the outdoor air temperature was about $30\text{--}35^{\circ}\text{C}$ and the relative humidity of the outdoor air was 80–95%). The artificial climate chamber was specially designed to simulate a domestic environment, as shown in Fig. 2.

The indoor air temperature range considered to be neutral typically falls between 24 and 28°C [39]. To obtain a wide range of thermal sensation votes, the air-conditioned room temperatures were set at 23°C , 26°C , and 29°C . While some individuals may prefer to use A/C in the ventilation mode instead of cooling mode to make them feel cooler, the indoor environment at 32°C was established to simulate conditions

Table 1
Skin temperature measuring instruments.

Instruments	Range	Resolution	Thermal sensitivity	Accuracy
FLIR T-460	-20-1500 °C	$320 (\text{V}) \times 240 (\text{H})$ pixels	<45 mK (under 30 °C ambient environment)	$\pm 1^{\circ}\text{C}$ or $\pm 1\%$ of readings, whichever is greater
Pyrobutton	-20-85 °C	-	0.005 °C	0.1 °C

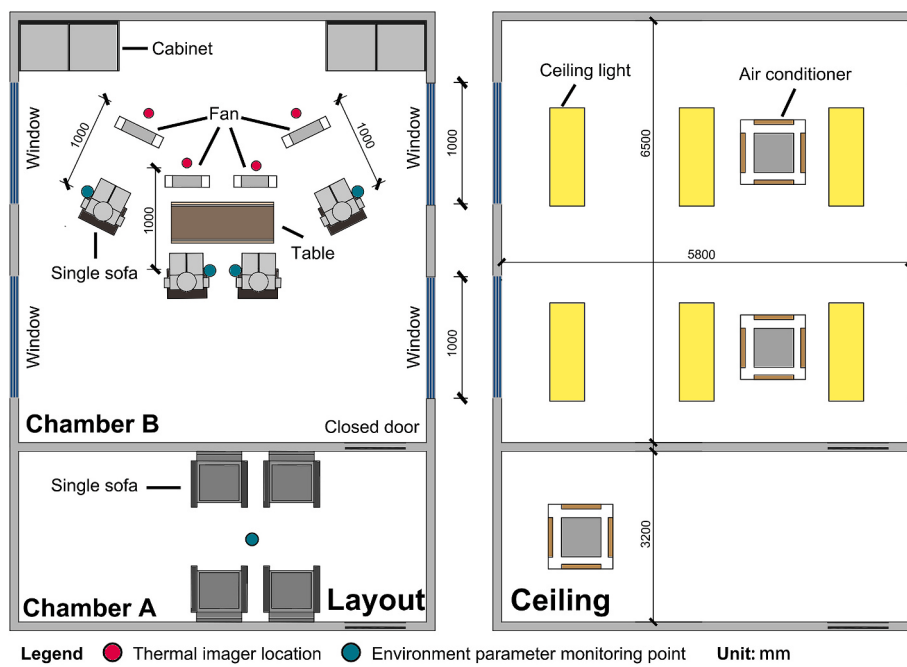


Fig. 2. The layout of climate chamber.

without A/C cooling during summer. Existing study has suggested that the recommended indoor air velocity can exceed the traditional value of 0.3 m/s, reaching up to 1.3 m/s or higher [40–42]. To account for this, the study utilized air velocity as an additional environmental variable, achieved by placing a fan in front of the subject. By changing the distance from the subject and the power of the fan, air velocities of 0 m/s, 0.4 m/s, 0.8 m/s, 1.6 m/s, and 2.4 m/s can be provided to the subject area. Referring to existing studies, three levels of air velocity were designed for each air temperature (as the air temperature rises, the upper limit of the designed air velocity rises) [41,42]. The designed experimental conditions, along with the corresponding actual environmental parameters, are presented in Table 2. Random number generator was used to generate a random sequence for the experiment conditions to minimize the impact of order effects [43]. The actual environmental parameters to which the subjects were exposed during the experiment were collected through data from the monitoring points (1.2 m above the ground). The instruments utilized for measuring environmental parameters at the measuring points are presented in Table 3. It is noted that the ceiling-installed A/C employed a low-speed air supply and the air supply angle was strategically adjusted to prevent direct airflow into the subject's area to minimize the potential interference of airflow from the A/C.

Subject sample size was calculated strictly according to G*power

Table 3
Environment parameters measuring instruments.

Parameters	Instrument	Range	Accuracy
Indoor air temperature	Swema 03+, SWEMA AB, Sweden	10–40 °C	±0.2 °C
Indoor air velocity	Swema 03+, SWEMA AB, Sweden	0–10 m/s	±0.01 m/s
Black globe temperature	Swema 05, SWEMA AB, Sweden	0–50 °C	±0.1 °C
Relative humidity	TR-76Ui, T&D CO., Japan	10–95%	±5%

software and ANOVA (repeated measures, within-between interaction) was selected as statistical test. The effect size took 0.25 (medium effect size), α error took 0.05, 1- β error took 0.8, number of groups took 2 [44]. The calculated minimum total sample size was 24. Ultimately, a sample size of 28 was chosen. One male subject withdrew from the study due to personal reasons, resulting in a final sample size of 27 subjects. All subjects were healthy college students from Shanghai Jiao Tong University who had resided in Shanghai for over five years on a long-term basis (refer to Table 4 for information). Every subject's body mass index (BMI) rate in the normal range [45]. The subjects wore summer clothing, which consisted of short-sleeved T-shirts, trousers, socks, and

Table 2
Experimental designed and measured parameters.

Number	Indoor air temperature (°C)		Air velocity (m/s)		Relative humidity (%)		Black globe temperature (°C)	
	Designed value	Measured value	Designed value	Measured value	Measured value	Measured value	Measured value	Measured value
1	23	23.2 ± 0.3	0.4	0.37 ± 0.09	56 ± 2	23.7 ± 0.3		
2	26	26.1 ± 0.3	0	0.07 ± 0.06	60 ± 1	26.4 ± 0.2		
3	29	28.7 ± 0.4	0.8	0.79 ± 0.09	61 ± 3	29.4 ± 0.4		
4	32	31.9 ± 0.3	1.6	1.59 ± 0.10	65 ± 1	32.8 ± 0.3		
5	29	28.9 ± 0.2	1.6	1.56 ± 0.04	60 ± 1	29.0 ± 0.4		
6	26	25.9 ± 0.2	1.6	1.59 ± 0.05	64 ± 3	26.2 ± 0.3		
7	23	22.7 ± 0.2	0.8	0.75 ± 0.06	50 ± 3	22.8 ± 0.2		
8	29	29.3 ± 0.3	0	0.07 ± 0.04	63 ± 2	29.5 ± 0.3		
9	23	22.8 ± 0.2	0	0.09 ± 0.03	55 ± 3	23.1 ± 0.4		
10	32	32.3 ± 0.2	0	0.06 ± 0.04	64 ± 2	32.6 ± 0.3		
11	32	31.8 ± 0.2	2.4	2.35 ± 0.10	63 ± 1	32.5 ± 0.2		
12	26	25.7 ± 0.2	0.8	0.78 ± 0.06	58 ± 2	25.8 ± 0.3		

Table 4
Subjects' information.

Gender	Number	Age	BMI	Number of years living in this area
Male	13	23.1 ± 4.3	22.2 ± 2.3	5–10 years
Female	14	24.4 ± 4.9	20.1 ± 1.3	5–10 years

slippers, resulting in a clothing level of 0.50 clo. The female subjects in this experiment had shoulder-length hair or ponytails, while the male had short hair and no facial hair. All subjects had their heads, forearms and hands uncovered by clothing, and surface temperatures could be collected directly by thermal imaging. Each subject was required to participate in all experimental conditions in sequence listed in Table 2, with a rest period of at least 24 h between each condition to eliminate any potential sequential effects. To mitigate the effects of circadian rhythms, participants were instructed to maintain a consistent sleep-wake schedule for one week preceding the experimental period and partake in the experiment at the same time each day until the end of all experiments [46]. Subjects were instructed to refrain from consuming caffeine, alcohol, and engaging in intense physical activity prior to the experiment. The experiment was approved by the Science and Technology Ethics Committee of the university. Verbal and written informed consent were obtained from each subject prior to their participation in each experiment.

The experimental procedure was conducted with each condition session lasting 90 min, consisting of a 30-min pre-experimental adaptation period followed by a 60-min experimental period (depicted in Fig. 3). The experiment was conducted with four subjects participating simultaneously. During the adaptation period, the subjects were allowed to rest in chamber A with an indoor temperature of 26 °C and an air velocity of less than 0.1 m/s to ensure the elimination of any prior thermal experiences. Additionally, the experimental procedure was described in detail to the subjects before the experiment. After the adaptation, the subjects were moved to the chamber B for the formal experiment. The subjects were required to complete the e-questionnaire at the 30th and 60th minute while also undergoing thermal imaging of the head, forearm, and hand dorsum from a distance of 1 m. The ASH-RAE 7-point TSV scale was used for the thermal sensation vote, ranging from "cold" (-3) to "hot" (3), and the subjects were instructed to use a slider to select the value that best represented their thermal sensation with one decimal place precision. During the experiment, subjects were allowed to engage in activities such as reading and using their mobile phones, which maintained an approximate metabolic rate of 1.1 MET.

2.3. Skin temperature extraction at different imaging views

The FLIR T-460 thermal imager utilized in this study has the capability to generate both Visual and Thermal images, which proved to be advantageous in accurately extracting the temperature information

required for the study. The imaging views utilized and the corresponding temperature information gathered are presented in Table 5. Notably, based on the findings of Tian et al. [32], the temperature variation between the symmetric positions on the left and right sides of the human head is minimal. Therefore, the lateral view imaging only targeted one side of the subject for imaging. In addition to the temperature data collected directly, derived data such as the minimum, maximum, the range and standard deviation of the temperature differences between

Table 5

The zone where the thermal camera can extract temperature at different imaging views.

Image capture view ^a	Data collection Zone	Derived data
Frontal face	Zone 1: Forehead Zone 2: Cheek Zone 3: Nose Zone 4: Mouth	Maximum, Minimum, Mean, Range of the temperature differences, Standard deviation of the temperature differences
Lateral face	Zone 1: Forehead Zone 2: Cheek Zone 3: Nose Zone 4: Ear helix	Maximum, Minimum, Mean, Range of the temperature differences, Standard deviation of the temperature differences
Top of the head	Zone 1: Overhead	–
Forearm/ Hand dorsum	Zone 1: Forearm Zone 2: Hand dorsum	–

^a The images included in this table are intended to illustrate various imaging perspectives and do not contain any identifying information or data.

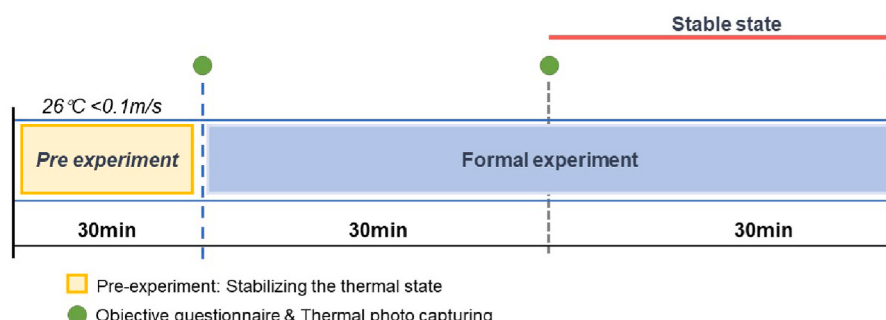


Fig. 3. Detail procedure of the experiment.

zones were also utilized.

The process of extracting skin temperature is illustrated in Fig. 4 and is explained as follows: Firstly, a visual image is generated by the FLIR camera upon capturing the subject, which is then used for the subsequent stages in face mesh generation. Secondly, a thermal image is generated, producing a raw image with temperature information. Thirdly, face mesh generation involves recognizing 468 3D facial feature points on faces captured from visible images using MediaPipe, an open-source machine learning framework, and OpenCV library [47]. The feature points are extracted by connecting the regions to form closed zones, which are positioned in the thermal image to determine the zones where temperature information is collected. It should be noted that the temperature of the ear is only collected from the ear helix. Finally, the mean temperature of each zone is extracted from the FLIR thermal images based on the detected key points. The extracted data is then processed to obtain the derived data. For this experiment, a total of 622 paired samples of subjective sensation vote-thermal imaging data were obtained from 27 subjects, where 502 paired samples were used in building the model, and 120 samples (60 each for males and females) were used for testing the model.

3. Two-stage model concept

Several subject experiments have found linear correlation between skin temperature and thermal sensation [48–50]. However, data collected in this study revealed that the skin temperature of different zones captured did not have a well linear relationship with thermal sensation (See Supplementary Material S2 for subject thermal sensations and extracted skin temperatures for all experimental conditions). For instance, Fig. 5(a) and Fig. 5(b) illustrate the connection between thermal sensation and mean frontal facial temperature ($T_{F\text{-Mean}}$) values acquired from frontal imaging. In this study, neutral thermal sensation vote ($-0.5 < TSV < +0.5$) corresponds to a wider temperature range, resulting in a distribution of sample points that resembles a flipped "S-shape". Similar temperature distribution patterns were observed in other zones, consistent with the findings of Tian et al. [32]. Upon separating the samples with a neutral thermal sensation, well linear fits of non-neutral thermal sensation to skin temperature were observed (as shown in Fig. 5(c) and (d)). Two-stage modelling method involves classifying the data first and then performing regression, rather than relying solely on either classification or regression [51,52]. This approach could improve the accuracy of the predictions, as the characteristics of a subset can be better fitted during the regression stage [51, 52]. Therefore, the two-stage modelling method is adopted in this study.

Two-stage model was employed that first categorized thermal sensations into three classes: "Cool side sensation ($TSV \leq -0.5$)", "Warm side sensation ($TSV \geq 0.5$)", and "Neutral sensation ($0.5 > TSV > -0.5$)". After the completion of the three-classification task, the subsequent step involves conducting a regression analysis of the non-neutral thermal sensation ("Cool side sensation" and "Warm side sensation") with the imaging surface temperature to calculate the specific non-neutral thermal sensation values.

Machine learning classifiers are a subset of algorithms within the broader field of machine learning, specifically designed to classify input data into distinct categories or classes. These classifiers learn patterns and relationships from training data to make predictions on unseen data, thereby enabling the automation of decision-making processes in various applications [53]. Previous studies have demonstrated that machine learning classifiers are useful for classification tasks in indoor thermal sensation research [54–56]. Therefore, in this study, a machine learning classifier was employed to construct a three-classification model for thermal sensation, utilizing temperature information. The identification of the optimal features and algorithms was also undertaken. As this study aims to target practical applications rather than improve algorithm performance, five basic algorithms - Random Forest (RF), Logistic Regression (LR), Support Vector Classification (SVC), K-Neighbors algorithm (KNN), and Gaussian Naive Bayes (Gaussian NB)- were selected for model building based on existing literatures and the suitability of each algorithm [4,57–59]. Table 6 shows the hyperparameters involved in optimizing each algorithm. To determine the optimal hyperparameters for different algorithms, grid search and four-fold cross-validation were used. The classification accuracy, as calculated by Equation (1), was used to assess the model's performance in classification. It is determined by dividing the number of correctly predicted data points by the total number of data points.

$$\text{Accuracy} = \frac{\sum_{i=1}^3 (TP_i)}{\sum_{i=1}^3 (TP_i + FP_i + FN_i)} \quad (1)$$

In Equation (1), TP_i is the number of samples in class "I" that are predicted to be correct; FP_i is the number of samples that are predicted to be class "I", but are actually other classes; FN_i is the number of samples that are actually class "I", but are predicted to be other classes.

By integrating the trained classifier with the regression model, a comprehensive two-stage model for assessing human thermal sensation across multiple perspectives is established. The evaluation of the final model was performed on the test set using the mean absolute error (MAE) as the evaluation metric, as calculated by Equation (2). MAE

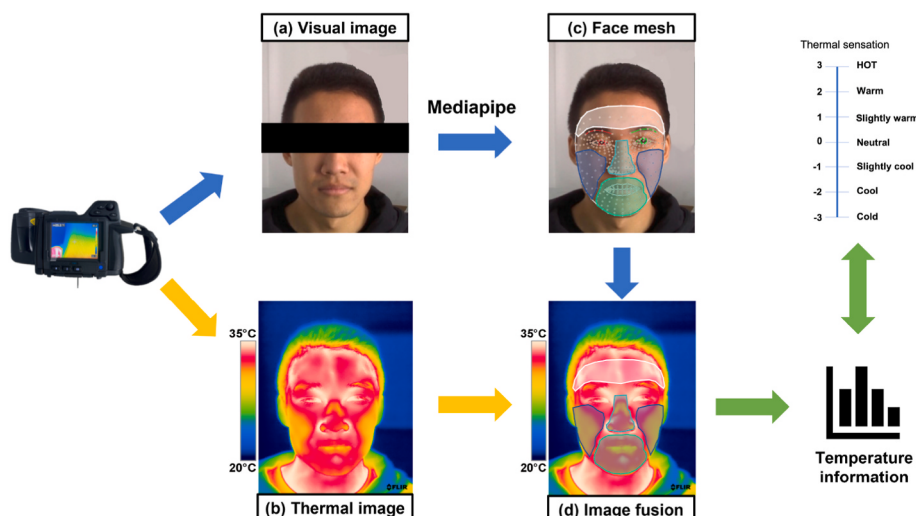


Fig. 4. The process of temperature extraction.

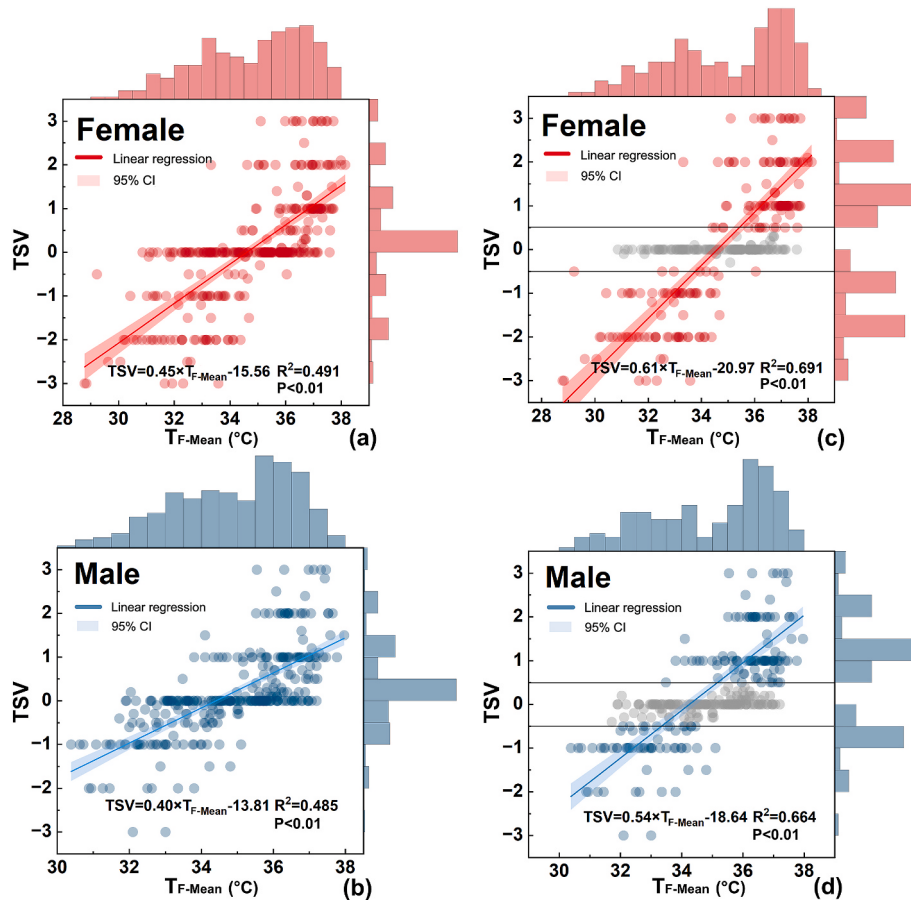


Fig. 5. Comparison of full linear fitting model and linear fitting model after separating neutral thermal sensation.

Table 6
The hyperparameters involved in the optimization.

Algorithm	Hyperparameters	Range
RF	n_estimators (numbers of trees in the forest)	1 to 100, with an interval of 1
	max_depth (the maximum depth of the tree)	1 to 20, with an interval of 1
LR	Solver	lbfgs, sag, newton-cg, saga
	C	0.001, 0.01, 0.1, 0.5, 1.0
SVC	Gamma	0.01, 0.1, 1, 10, 100
	Kernel	"poly", "rbf", "sigmoid"
KNN	algorithm	"auto", "ball_tree", "kd_tree", "brute"
Gaussian NB	-	-

provides insight into the mean error in assessing the thermal sensation of the final model, while also being resilient to the influence of outliers.

$$MAE = \frac{1}{n} \sum_{i=1}^n |y_i - \hat{y}_i| \quad (2)$$

In Equation (2), MAE is the mean absolute error (thermal sensation vote unit), n is the total number of observations in test set, y_i is the true TSV of the i^{th} observation, and \hat{y}_i is the predicted TSV of the i^{th} observation.

In practical applications, the thermal sensation is determined by inputting the surface temperature. If the thermal sensation is deemed neutral, a no-action command is outputted to the smart A/C. Conversely, if the thermal sensation deviates from the neutral state, the degree of deviation is computed and translated into different levels of set point change actions. The Scikit-learn machine learning library developed in

Python was used to invoke algorithms [53], while the Pandas library was used to perform the data processing [60].

4. Results

4.1. Modeling of three classes of thermal sensation classifiers

The thermal sensation classifier was trained using various temperature information and algorithms. The Pearson's correlation coefficient was computed between each temperature information, and the results are depicted in Fig. 6. Strong correlations ($r > 0.7$) were observed among the surface temperatures of each zone. It should be noted that many highly correlated features do not necessarily provide a greater amount of information. On the contrary, using more features may increase the susceptibility of the model to noise [61]. Therefore, this study did not utilize two or more skin temperatures as features simultaneously. The feature combinations in the thermal sensation classifier were categorized into four types: "single zone surface temperature", "single zone surface temperature and air velocity", "single zone surface temperature and air temperature", and "single zone surface temperature, air velocity, and air temperature".

The performance of all trained classifiers is presented in Tables S-3 to S-6 in the Supplementary Material S3. Table 7 highlights the best classifiers and their performance for each combination of features. Among all classifiers, the RF algorithm has shown the best performance in distinguishing the three classes of thermal sensations. Notably, the classification model achieved higher accuracy for males compared to females. In the case of the frontal face view, the classifier achieved an accuracy of 0.750–0.783 using only cheek temperature as input, while adding air temperature and airflow velocity to the features improved the model's

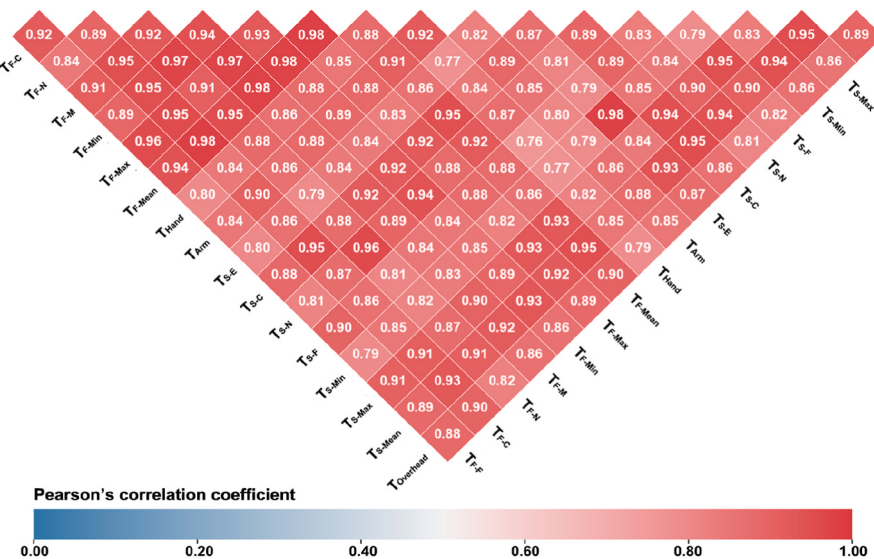


Fig. 6. Heat map of Pearson's correlation coefficient between variables.

accuracy up to 0.867 for males and 0.783 for females. For the lateral view of the face, the best classification performance achieved an accuracy of 0.767–0.817. For the overhead view, using overhead temperature distinguished the neutral/non-neutral thermal sensation well in both genders. For the forearm/hand dorsum view, the forearm surface temperature was preferred than hand. In building thermal sensation classification model via thermal imaging, the most optimal view is the frontal view of the face, followed by the lateral face, the top view of the head, and the view of the forearm/hand dorsum.

4.2. Modeling of non-neutral thermal sensation computational models

After distinguishing neutral and non-neutral thermal sensations, linear regression was used to fit the temperature data collected from different zones under different views to the non-neutral thermal sensations. The linear fitting results are shown in Fig. 7. The slope of the linear fit reflects the sensitivity of skin temperature to non-neutral thermal sensation. Overall, female head (including frontal face, lateral face, and top of the head) surface temperatures were found to be more sensitive to non-neutral thermal sensation than males. Among the temperature data collected by the thermal imager in frontal and lateral facial views, the minimum values of the four facial zones in males showed the best fit with non-neutral thermal sensation (with R^2 of 0.68 and 0.71, respectively), while the cheek temperature in females showed the best fit (with R^2 of 0.68 and 0.69, respectively). The overhead temperature collected by the top view thermography was also well correlated with non-neutral thermal sensation ($R^2 = 0.69$). The forearm surface temperature collected by thermal imaging was found to be the best indicator for assessing deviation from neutral thermal sensation in the forearm/hand dorsum view (with R^2 of 0.69 for males and 0.74 for females).

In addition, the data showed that the uniformity of temperature distribution in the head varied with changes in thermal sensation. The range and standard deviation of the temperature differences between different zones as measured from frontal and lateral facial views were used as indicators to evaluate temperature distribution uniformity. The study found that when the thermal sensation was −3 for females and −2 for males, the range of temperature differences in frontal facial temperatures (T_{F-ED}) were 6.6 ± 0.4 °C and 5.9 ± 0.7 °C, respectively. However, as the thermal sensation increased, the range of temperature differences in frontal facial temperatures decreased to 0.6 ± 0.2 °C and 0.4 ± 0.1 °C for females and males, respectively, indicating that the facial temperatures tended to become more uniform under "warm side" sensation. In contrast, under "cool side" sensation, the facial temperature

exhibited non-uniformity. A non-linear regression between the temperature distribution uniformity and non-neutral thermal sensation was established using the Levenberg-Marquardt algorithm, as shown in Fig. 8. When evaluating non-neutral thermal sensation based on the range of temperature difference between various facial zones in frontal thermal imaging, the R^2 values of the female and male models were 0.73 and 0.75, respectively, which were superior to the linear models established using skin temperature of a single zone. However, for lateral thermal imaging, the performance of evaluating non-neutral thermal sensation based on the range difference in temperature between different facial zones (T_{S-ED}) was slightly worse, with R^2 values of 0.51 and 0.72. The best models for calculating non-neutral thermal sensation using surface temperature under different thermal imaging views are listed in Table 8.

4.3. Thermal sensation model based on thermal imaging technology and its performance

A multi-perspective human thermal sensation evaluation model based on thermal imaging was established by combining thermal sensation classification model built on the RF algorithm with a non-neutral thermal sensation regression model. The model application process is illustrated in Fig. 9. Taking female users as an example, the imaging view of the user is first determined. If a frontal face image of the user can be captured, the cheek temperature is extracted and input into the trained RF classifier for thermal sensation classification. If non-neutral thermal sensation is output, the range of temperature differences between the four facial zones is calculated and input into the non-neutral thermal sensation calculation model to further calculate the deviation from neutral thermal sensation. Otherwise, the output is "neutral thermal sensation".

The proposed model was tested using test set. The output results of the proposed model was compared with the true thermal sensation votes of the subjects. The results are presented in Table 9. When the proposed model was applied to the male subset, the MAE of the output results ranged from 0.41 to 0.49, which did not exceed 0.5 thermal sensation units. Although the MAE of the output results for the female subset was slightly higher, ranging from 0.50 to 0.53.

5. Discussion

This study conducted subject experiments in an artificial climate chamber to collect surface temperature and subjective questionnaires

Table 7
Classifier performance for three-level thermal sensation classification.

View	Gender	Optimal features	Optimal hyperparameters	Accuracy
Frontal face	Female	T _{F-C}	n_estimators = 3, max_depth = 5	0.750
		T _{F-C} , T _{air}	n_estimators = 3, max_depth = 5	0.767
		T _{F-C} , V _{air}	n_estimators = 5, max_depth = 5	0.783
		T _{F-C} , T _{air} , V _{air}	n_estimators = 1, max_depth = 10	0.783
	Male	T _{F-C}	n_estimators = 3, max_depth = 8	0.783
		T _{F-C} , T _{air}	n_estimators = 19, max_depth = 3	0.833
		T _{F-C} , V _{air}	n_estimators = 30, max_depth = 2	0.833
		T _{F-Min} , T _{air} , V _{air}	n_estimators = 6, max_depth = 4	0.867
Lateral face	Female	T _{S-C}	n_estimators = 42, max_depth = 5	0.750
		T _{S-C} , T _{air}	n_estimators = 32, max_depth = 20	0.767
		T _{S-C} , V _{air}	n_estimators = 2, max_depth = 9	0.750
		T _{S-N} , T _{air} , V _{air}	n_estimators = 4, max_depth = 3	0.767
	Male	T _{S-Mean}	n_estimators = 6, max_depth = 4	0.783
		T _{S-C} , T _{air}	n_estimators = 7, max_depth = 4	0.817
		T _{S-Mean} , V _{air}	n_estimators = 22, max_depth = 5	0.817
		T _{S-Min} , T _{air} , V _{air}	n_estimators = 9, max_depth = 3	0.817
Top of the head	Female	T _{Overhead}	n_estimators = 5, max_depth = 6	0.700
		T _{Overhead} , T _{air}	n_estimators = 7, max_depth = 8	0.700
		T _{Overhead} , V _{air}	n_estimators = 33, max_depth = 8	0.733
		T _{Overhead} , T _{air} , V _{air}	n_estimators = 12, max_depth = 10	0.750
	Male	T _{Overhead}	n_estimators = 8, max_depth = 4	0.800
		T _{Overhead} , T _{air}	n_estimators = 14, max_depth = 4	0.800
		T _{Overhead} , V _{air}	n_estimators = 4, max_depth = 3	0.800
		T _{Overhead} , T _{air} , V _{air}	n_estimators = 1, max_depth = 4	0.833
Forearm/ Hand dorsum	Female	T _{Arm}	n_estimators = 7, max_depth = 10	0.717
		T _{Arm} , T _{air}	n_estimators = 2, max_depth = 2	0.700
		T _{Arm} , V _{air}	n_estimators = 5, max_depth = 2	0.683
		T _{Hand} , T _{air} , V _{air}	n_estimators = 66, max_depth = 6	0.767
	Male	T _{Arm}	n_estimators = 5, max_depth = 6	0.750
		T _{Arm} , T _{air}	n_estimators = 3, max_depth = 2	0.783
		T _{Arm} , V _{air}	n_estimators = 33, max_depth = 4	0.783
		T _{Arm} , T _{air} , V _{air}	n_estimators = 14, max_depth = 3	0.800

from subjects in four thermal imaging views. A human thermal sensation evaluation model suitable for different genders in different thermal imaging views was established.

Tian et al. [62] found that the temperature of the nose had the best correlation with thermal sensation compared to other body parts. In this study, it was observed that some subjects' nose temperature was lower than other locations when they felt cold, but this feature did not appear

in all subjects. When feeling cold, more subjects exhibited lower temperatures in their cheeks than in other zones. Combining the findings of both researches, this study suggests that the temperature range between different facial zones more accurately reflects human thermal sensation. Specifically, the more an occupant feels cold, the more uneven the facial temperature distribution becomes. This conclusion is consistent with previous researches [31,34]. The results of non-linear regression indicate that when the occupant experience a sensation of cold, the temperature difference between different frontal facial zones is approximately 2–3 °C. Non-linear regression of temperature range and non-neutral thermal sensation was found to be poor for thermal imaging from a lateral view. This may be due to the fact that zones with stable and high temperatures (e.g., the center of the forehead and the area around the mouth) are not captured in the lateral view imaging. This may result in a lower temperature range in the lateral imaging when the body is experiencing cold sensations. Furthermore, the ear temperature of female subjects captured by lateral imaging was not well-fitted to the non-neutral thermal sensation. This was due to the simulation of a domestic environment in an artificial climate chamber, which did not require female subjects to adhere to a specific hairstyle. Instead, all subjects were instructed to feel as relaxed as possible during the experiment. As a result, some female subjects' long hair obscured their ears before imaging, leading to elevated ear temperatures in their images. To ensure data validity, these data were removed, which had an impact on the regression results. Several studies have suggested that exposed hand surface temperature is an effective indicator of human thermal sensation [27,29,63], although our findings differ from this conclusion. This discrepancy could be attributed to the specific conditions of our study, which simulated a domestic environment where participants could their mobile phones (hands being in a near fist shape) during the experiment. They were only asked to stretch out their hands for imaging. Heat dissipation from mobile phones may impact hand surface temperature, resulting in an inaccurate reflection of the subjects' thermal sensation. This study identified that assessing thermal sensation using the surface temperature of the top of the head shows some promise. This may be because the surface temperature of the hair better reflects the ambient temperature and air velocity than the skin temperature. However, more research is required to support this. This is because the sensitivity of head temperature to thermal sensation could be influenced by hair style. In our study, most female participants had shoulder-length hair or ponytails, and male participants had short hair. Therefore, this study assumes that the thickness of the overhead hair is roughly the same for participants of the same gender.

The question of whether there are gender differences in both physiological and psychological responses to indoor environments remains a current research focus. Some studies have indicated that psychological perception may not differ significantly between males and females in the same environment, but there may be significant differences in skin temperature, suggesting that the response of skin temperature to thermal sensation may differ between genders [64–67]. Gender differences observed in the studies exploring the response of human limb skin temperature to thermal sensation are often attributed to differences in fat thickness, hormone levels, and body surface area between genders [68]. This study found that there are also gender differences in the sensitivity of psychological perception to changes in facial skin temperature. Specifically, female have been found to generally exhibit higher facial temperatures than male when experiencing cold sensations in cold environments, suggesting that female may perceive cold sensations earlier than male. This also results in lower minimum values of male facial temperature than female for the same cold sensation. Since the highest values tend to occur around the mouth where the temperature is relatively stable, it makes the facial temperature distribution more uneven in male under cold sensation. Currently, it is not available for us to give sufficient explanations that can explain the gender differences in facial temperature with the same cold sensation. However, it may be related to the involvement of estrogen in thermoregulatory

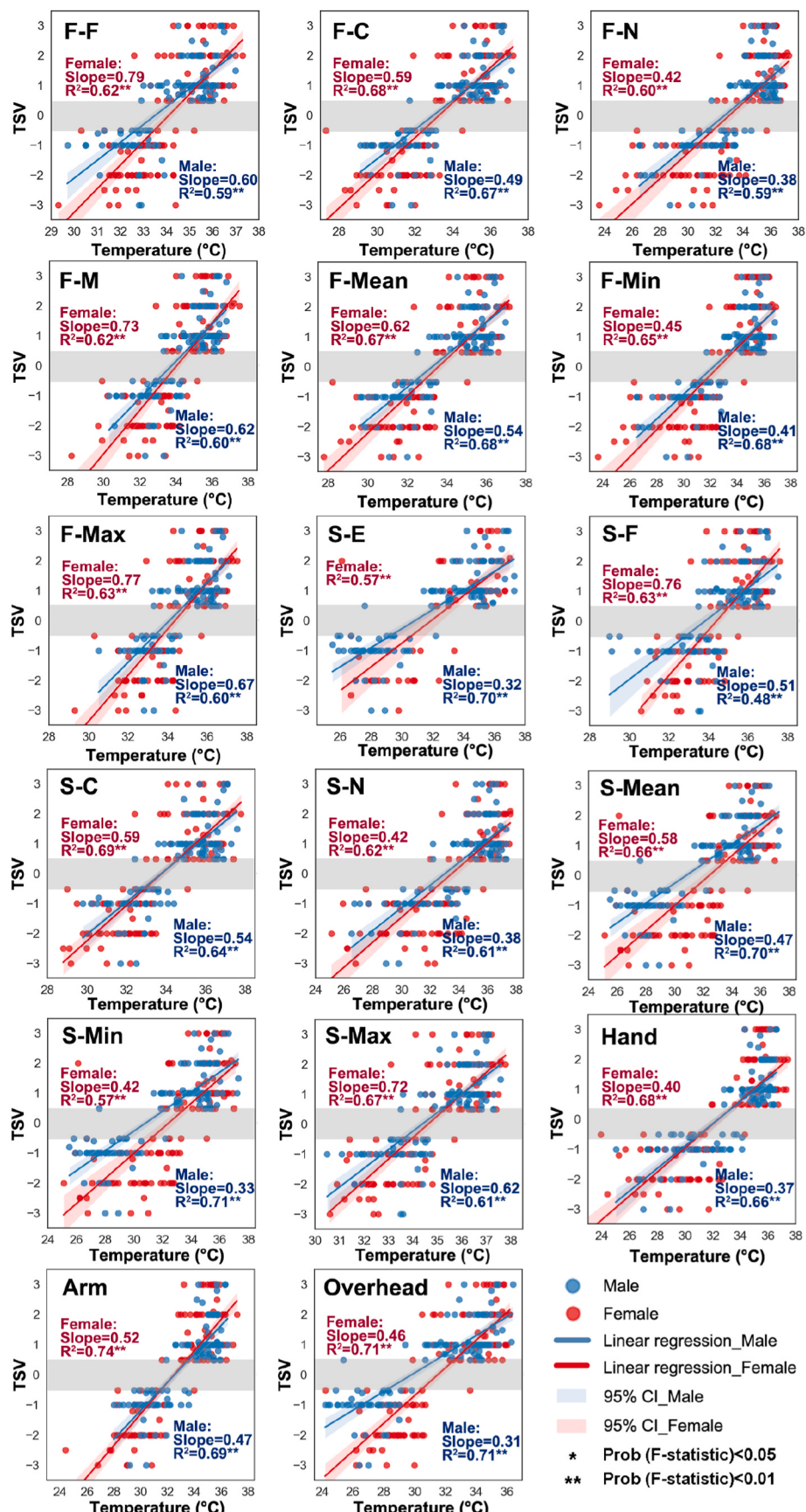


Fig. 7. Linear fitting of non-neutral thermal sensation to the temperature captured by thermal camera.

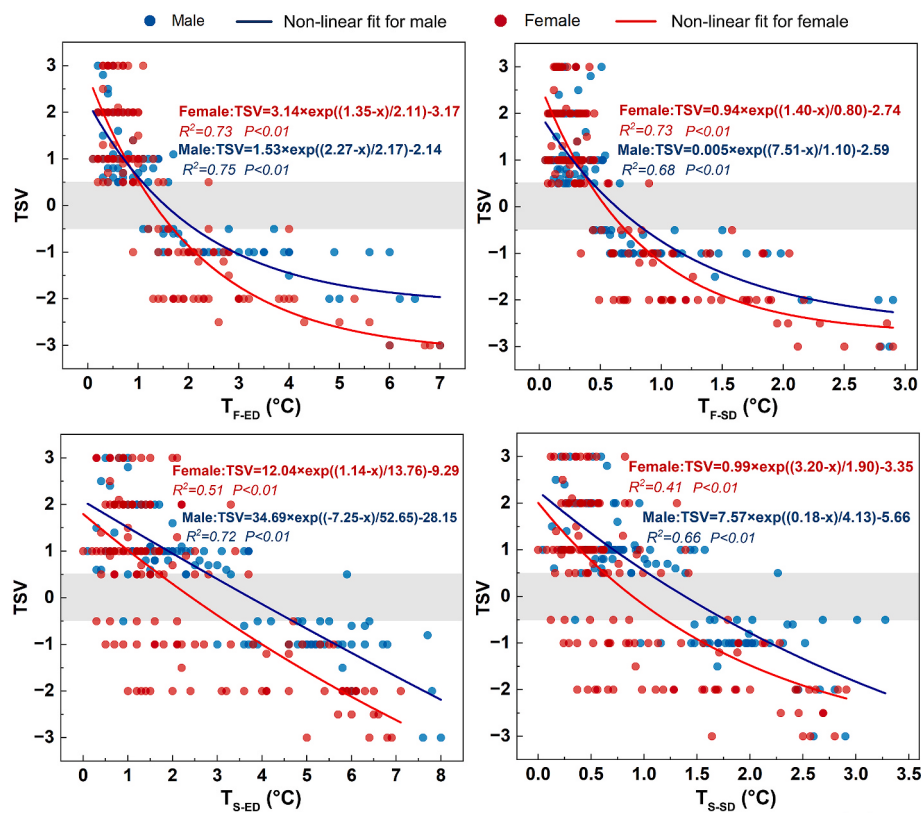


Fig. 8. Non-linear regression between non-neutral thermal sensation and facial temperature non-uniformity in frontal and lateral view.

Table 8

Optimal fitting models for non-neutral thermal sensation and surface thermographic temperature at different views.

View	Gender	Optimal model	R ²	P-Value
Frontal face	Female	$TSV = 3.14 \times \exp\left(\frac{1.35 - T_{F-ED}}{2.11}\right) - 3.17$	0.73	<0.01
	Male	$TSV = 1.53 \times \exp\left(\frac{2.27 - T_{F-ED}}{2.17}\right) - 2.14$	0.75	<0.01
Lateral face	Female	$TSV = -20.10 + 0.59 \times T_{S-C}$	0.69	<0.01
	Male	$TSV = 34.69 \times \exp\left(\frac{-7.25 - T_{S-ED}}{52.65}\right) - 28.15$	0.72	<0.01
Top of the head	Female	$TSV = -14.51 + 0.46 \times T_{Overhead}$	0.71	<0.01
Male		$TSV = -9.24 + 0.31 \times T_{Overhead}$	0.71	<0.01
Forearm/Hand dorsum	Female	$TSV = -16.99 + 0.52 \times T_{Arm}$	0.74	<0.01
Male		$TSV = -15.32 + 0.47 \times T_{Arm}$	0.69	<0.01

mechanisms that impede the flow of blood to the skin surface [17]. These response sensitivity differences of thermal sensation to skin temperature suggest that collecting facial temperature by thermal imager for thermal sensation assessment requires distinction between genders to enhance assessment accuracy.

It is worth noting that although the correlation between skin temperature and thermal sensation is well-established for most people, a minority of individuals exhibit a distinct skin temperature response to changes in their thermal environment. Fig. 10 displays the relationship between cheek temperature and thermal sensation for three subjects. Subject #8 demonstrated response characteristics consistent with most of the subjects. However, subject #6 voted most of the environments as

having neutral thermal sensation, despite great variations in cheek temperature across different conditions. Therefore, the proposed model is unsuitable for this subject. Subject #12 displayed a markedly different response characteristic, with a highly correlated linear relationship between thermal sensation and cheek temperature. In other words, this subject's cheek temperature showed significant sensitivity to even minor changes in thermal sensation. This model is based on a certain number of subjects, aimed at evaluating individual thermal sensation from the perspective of physiological temperature, which is applicable to most people. However, considering the individual characteristics of a small number of subjects, future work can collect data on special individuals and use reinforcement learning algorithms and incremental learning algorithms to make the model more individualized [22].

The preliminary results have demonstrated the feasibility and potential of the established thermal imaging-based thermal sensation assessment model. However, the proposed model was developed based on steady-state thermographic temperature and overall thermal sensation votes. The performance of the model for transient environments is still to be tested. The proposed framework may be well adapted to transient environments by incorporating time-series factors, such as rate of temperature change. In addition, it should be noted that important user-specific variables other than gender still have a potential impact on the accuracy and generalizability of our model. The subjects in this study were all from climates with hot and humid summers and had lived there for at least five years. People living in different climates may exhibit different thermal sensations even under the same conditions. For instance, individuals from colder climates may have a higher tolerance for low temperatures [69]. The variability in climate adaptation may pose a challenge to the application of proposed model in other climatic zones. In addition, the model was built based on data from subjects with a BMI of 20–25 (normal weight). Due to the insulating effect of adipose tissue, people with higher body fat content are more likely to feel warm than those with lower body fat content [70]. This suggests that the relationship between skin temperature and thermal sensation in

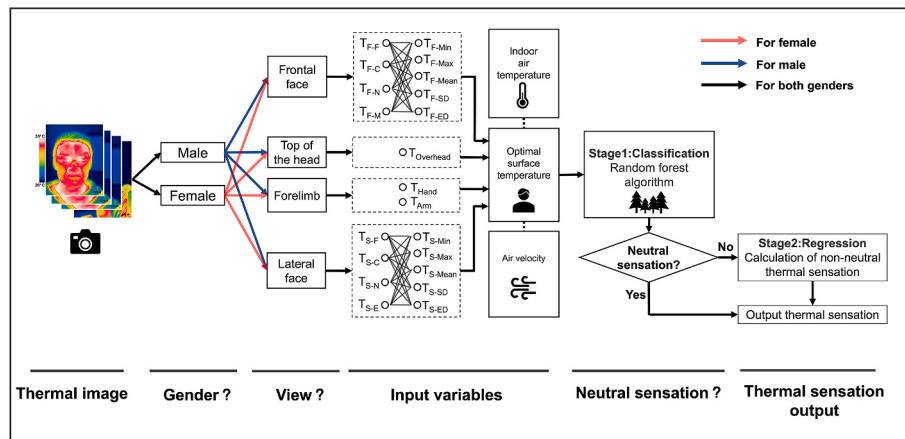


Fig. 9. Application process of thermal sensation assessment model based on data captured by thermal imager.

Table 9

The MAE of the proposed model for the test set.

Gender	View	MAE (thermal sensation unit)
Female	Frontal face	0.50
	Lateral face	0.51
	Top of the head	0.53
	Forearm/Hand dorsum	0.53
Male	Frontal face	0.41
	Lateral face	0.45
	Top of the head	0.41
	Forearm/Hand dorsum	0.49

individuals with obesity or leanness may not be applicable to the model proposed in this study. Age is another critical factor that can influence an individual's thermal sensation. As people age, their ability to perceive and respond to thermal environment may decline due to reduced metabolic rate, decreased blood flow, and impaired thermoregulatory mechanisms [71,72]. This suggests that proposed model may not be equally accurate for individuals across different age groups. Incorporating these user-specific variables into the model may improve predictive accuracy and generalization.

6. Practical applications and future perspective

This study is a preliminary exploration of the application of thermal imaging technology in A/C systems to achieve whole-house smart

control with the goal of catering to the thermal demands of users. The results obtained can provide reference for the installation position of thermal imaging sensors, the setting of temperature acquisition zones, and thermal sensation calculation. In practical applications, the thermal imaging sensor can be installed either on the wall surface (as depicted in Fig. 11(a)) or directly integrated into a split A/C unit (as illustrated in Fig. 11(b)) to achieve the desired optimal imaging view. The data acquisition system (as shown in Fig. 11(c)) facilitates the real-time extraction of the surface temperature to compute thermal sensation, which subsequently triggers the automatic adjustment of the A/C set point. This study found that the best performance in thermal sensation evaluation was achieved when surface temperature, indoor air temperature, and air velocity were used as model features. However, it should be noted that compared to air temperature, high-precision sensors used to measure air velocity are expensive and difficult to incorporate into building automation equipment for daily use. Although using only specific surface temperature and indoor air temperature as features for thermal sensation evaluation may result in a loss of accuracy, this model may be more feasible.

Currently, there are other issues with the practical application of A/C automatic control based on thermal imaging. Our research team has also begun to investigate these issues. The first problem is the imbalance between the cost, resolution, and accuracy of the thermal imaging sensor. The thermal camera used in our study was the FLIR T-460, which is an expensive professional instrument. After validation, this camera was found to have high accuracy and stability. However, in practical applications, integrating such expensive professional instrument into A/

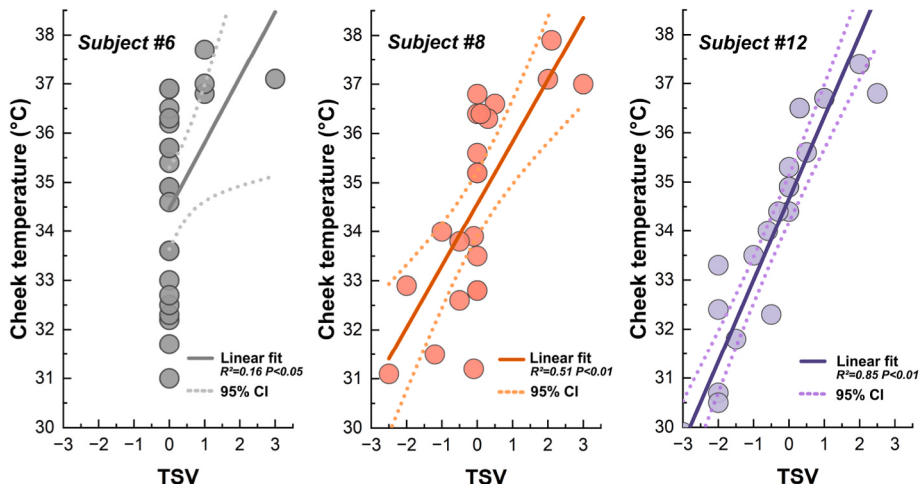


Fig. 10. Individual-specific differences in the correlation between thermal sensation and frontal cheek temperature.

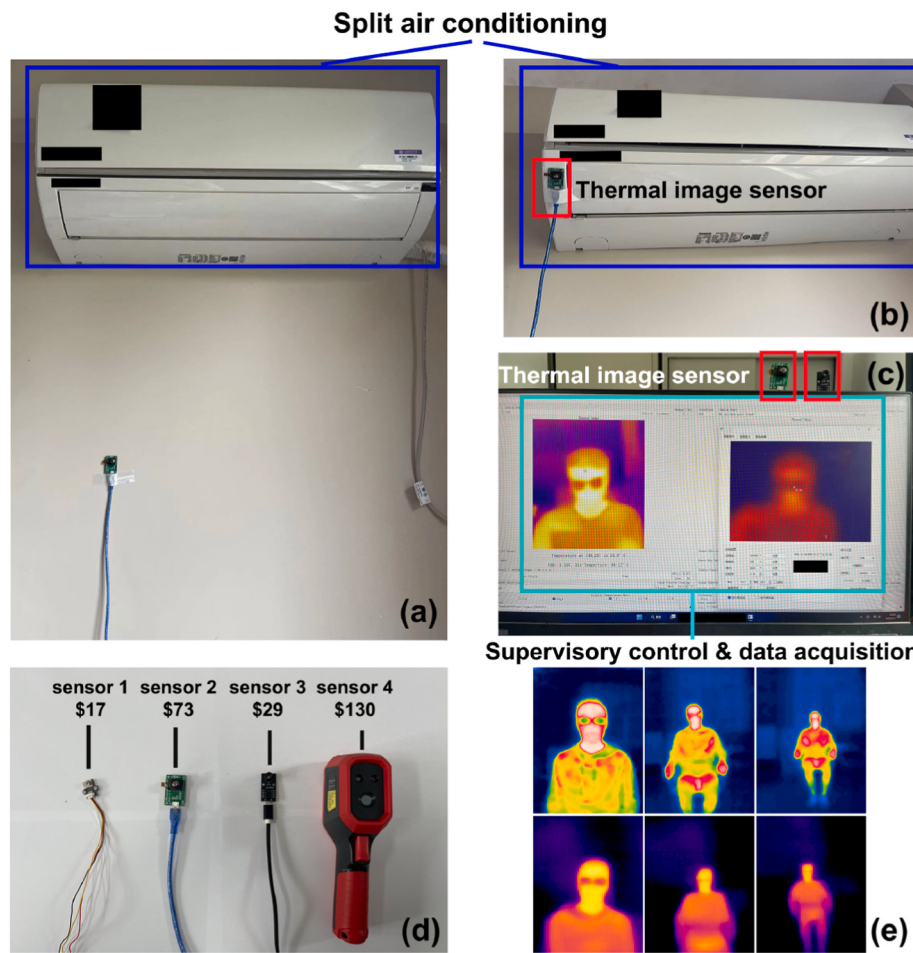


Fig. 11. Practical applications and the next steps for future researches.

C is not feasible. The next step of the research could involve comparing the performance of various sensors (as shown in Fig. 11(d)). Additionally, the impact of imaging distance on imaging accuracy also needs to be further clarified. Wu et al. [29] have pointed out that the FLIR high-performance thermal imager is minimally affected by distance when imaging within 3 m. Thus, the conclusion of this study is not significantly influenced by the imaging distance within 3 m. However, for cheaper sensors, distance may be an important factor (as shown in Fig. 11(e)). Therefore, it is necessary to explore the differences in readings of the same sensor at different imaging distances and introduce correction factors. This may make future practical applications more feasible. Lastly, the practical application of the model in a multi-person space is worth exploring. By capturing the characteristic temperatures of multiple people and combining optimization theory, adjusting the A/C set point to cater to the overall thermal demand of a group of people may be a solution.

7. Conclusions

Through the subject experiment, this study combined machine learning classification algorithms and regression algorithms to analyze the surface temperature collection zones that accurately reflect thermal sensation under different imaging views. Moreover, thermal sensation evaluation two-stage models were established for users of different genders, which are suitable for various thermal imaging views. The main conclusions are as follows:

1. In assessing human thermal sensation via thermal imaging, the most optimal view is the frontal face, followed by the lateral face, the top of the head, and the forearm/hand dorsum.
2. The range of temperature differences between facial zones, cheek surface temperature, overhead surface temperature, and forearm surface temperature can be used as indicators for assessing the degree of deviation from neutral thermal sensation.
3. By using the random forest algorithm, using only the cheek temperature from frontal face imaging as a feature can achieve an accuracy rate of 75.0%–78.3% for three-level thermal sensation classification. Adding indoor air temperature and air velocity to the features can increase the accuracy of the classification model to a maximum of 86.7%.
4. The proposed thermal sensation evaluation two-stage model based on thermal imaging has a MAE of 0.41–0.49 thermal sensation units for male and 0.50–0.53 thermal sensation units for female.

CRediT authorship contribution statement

Junmeng Lyu: Writing – original draft, Investigation, Formal analysis, Data curation. **Heng Du:** Writing – review & editing. **Zisheng Zhao:** Writing – original draft, Conceptualization. **Yongxiang Shi:** Writing – review & editing. **Bo Wang:** Writing – review & editing. **Zhiwei Lian:** Writing – review & editing, Methodology, Funding acquisition, Conceptualization.

Declaration of competing interest

The authors declare that they have no known competing financial

interests or personal relationships that could have appeared to influence the work reported in this paper.

Data availability

Data will be made available on request.

Acknowledgements

This work is supported by the National Key R&D Program of China (2022YFC3803201).

Appendix A. Supplementary data

Supplementary data to this article can be found online at <https://doi.org/10.1016/j.buildenv.2023.110405>.

References

- [1] A. Allouhi, Y. El Fouih, T. Kousksou, A. Jamil, Y. Zeraouli, Y. Mourad, Energy consumption and efficiency in buildings: current status and future trends, *J. Clean. Prod.* 109 (2015) 118–130, <https://doi.org/10.1016/j.jclepro.2015.05.139>.
- [2] Z. Zhang, R. Gao, Y. Liu, M. Liu, Y. Wang, W. Zhu, L. Zhou, A. Li, Smart air supply terminal for floor-standing room air conditioners based on the identification of human positions, *Build. Environ.* 202 (2021), 108041, <https://doi.org/10.1016/j.buildenv.2021.108041>.
- [3] ASHRAE, ANSI/ASHRAE Standard 55-2020: Thermal Environmental Conditions for Human Occupancy, 2020.
- [4] J. Lyu, J. Li, Z. Zhao, X. Miao, H. Du, D. Lai, Y. Yang, Z. Lian, How do people set air conditioning temperature setpoint in urban domestic-Behavior model in Chinese three climate zones based on historical usage data, *Energy Build.* 284 (2023), 112856, <https://doi.org/10.1016/j.enbuild.2023.112856>.
- [5] F. Hou, J. Ma, H.H.L. Kwok, J.C.P. Cheng, Prediction and optimization of thermal comfort, IAQ and energy consumption of typical air-conditioned rooms based on a hybrid prediction model, *Build. Environ.* 225 (2022), 109576, <https://doi.org/10.1016/j.buildenv.2022.109576>.
- [6] X. Wang, S. Liu, L. Xiong, D. Wu, Y. Zhang, Research on intelligent regulation of air conditioning energy saving based on human thermal comfort, *J. Ambient Intell. Hum. Comput.* (2021), <https://doi.org/10.1007/s12652-021-02999-z>.
- [7] P.O. Fanger, Thermal Comfort. Analysis and Applications in Environmental engineering., *Thermal Comfort. Analysis and Applications in Environmental Engineering*, 1970.
- [8] H. Du, Z. Lian, D. Lai, L. Duanmu, Y. Zhai, B. Cao, Y. Zhang, X. Zhou, Z. Wang, X. Zhang, Z. Hou, Evaluation of the accuracy of PMV and its several revised models using the Chinese thermal comfort Database, *Energy Build.* 271 (2022), 112334, <https://doi.org/10.1016/j.enbuild.2022.112334>.
- [9] T. Chaudhuri, Y.C. Soh, H. Li, L. Xie, Machine learning based prediction of thermal comfort in buildings of equatorial Singapore, in: IEEE International Conference on Smart Grid and Smart Cities, ICSGSC, 2017, pp. 72–77, <https://doi.org/10.1109/ICSGSC.2017.8038552>, 2017.
- [10] H. Na, J.-H. Choi, H. Kim, T. Kim, Development of a human metabolic rate prediction model based on the use of Kinect-camera generated visual data-driven approaches, *Build. Environ.* 160 (2019), 106216, <https://doi.org/10.1016/j.buildenv.2019.106216>.
- [11] B. Yang, X. Cheng, D. Dai, T. Olofsson, H. Li, A. Meier, Real-time and contactless measurements of thermal discomfort based on human poses for energy efficient control of buildings, *Build. Environ.* 162 (2019), 106284, <https://doi.org/10.1016/j.enbuild.2019.106284>.
- [12] M. Luo, K. Jiang, J. Wang, W. Feng, L. Ma, X. Shi, X. Zhou, Data-driven thermal preference prediction model with embodied air-conditioning sensors and historical usage behaviors, *Build. Environ.* 220 (2022), 109269, <https://doi.org/10.1016/j.buildenv.2022.109269>.
- [13] Z. Wang, R. Matsuhashi, H. Onodera, Intrusive and non-intrusive early warning systems for thermal discomfort by analysis of body surface temperature, *Appl. Energy* 329 (2023), 120283, <https://doi.org/10.1016/j.apenergy.2022.120283>.
- [14] Z. Wang, R. Matsuhashi, H. Onodera, Towards wearable thermal comfort assessment framework by analysis of heart rate variability, *Build. Environ.* 223 (2022), 109504, <https://doi.org/10.1016/j.buildenv.2022.109504>.
- [15] E.R. Nadel, R.W. Bullard, J.A. Stolwijk, Importance of skin temperature in the regulation of sweating, *J. Appl. Physiol.* 31 (1971) 80–87, <https://doi.org/10.1152/jappl.1971.31.1.80>.
- [16] H. Kaciuba-Uscilko, R. Grucza, Gender differences in thermoregulation, *Curr. Opin. Clin. Nutr. Metab. Care* 4 (2001). https://journals.lww.com/co-clinicalnutrition/Fulltext/2001/11000/Gender_differences_in_thermoregulation.12.aspx.
- [17] Y. Uchida, K. Nagashima, S. Marui, Estrogenic modulation of female thermoregulatory behavior in a cold environment, *J Phys Fit Sports Med* 5 (2016) 77–80, <https://doi.org/10.7600/jpfsm.5.77>.
- [18] N. Charkoudian, Skin blood flow in adult human thermoregulation: how it works, when it does not, and why, *Mayo Clin. Proc.* 78 (2003) 603–612, <https://doi.org/10.4065/78.5.603>.
- [19] D.J. Yeom, F. Delogu, Local body skin temperature-driven thermal sensation predictive model for the occupant's optimum productivity, *Build. Environ.* 204 (2021), 108196, <https://doi.org/10.1016/j.buildenv.2021.108196>.
- [20] C. Dai, H. Zhang, E. Arens, Z. Lian, Machine learning approaches to predict thermal demands using skin temperatures: steady-state conditions, *Build. Environ.* 114 (2017) 1–10, <https://doi.org/10.1016/j.buildenv.2016.12.005>.
- [21] T. Chaudhuri, Y.C. Soh, H. Li, L. Xie, Machine learning driven personal comfort prediction by wearable sensing of pulse rate and skin temperature, *Build. Environ.* 170 (2020), 106615, <https://doi.org/10.1016/j.buildenv.2019.106615>.
- [22] J. Xie, H. Li, C. Li, J. Zhang, M. Luo, Review on occupant-centric thermal comfort sensing, predicting, and controlling, *Energy Build.* 226 (2020), 110392, <https://doi.org/10.1016/j.enbuild.2020.110392>.
- [23] B. Yang, X. Li, Y. Hou, A. Meier, X. Cheng, J.-H. Choi, F. Wang, H. Wang, A. Wagner, D. Yan, A. Li, T. Olofsson, H. Li, Non-invasive (non-contact) measurements of human thermal physiology signals and thermal comfort/discomfort poses -A review, *Energy Build.* 224 (2020), 110261, <https://doi.org/10.1016/j.enbuild.2020.110261>.
- [24] P.V.K. Yadav, I. Yadav, B. Ajitha, A. Rajasekar, S. Gupta, Y. Ashok Kumar Reddy, Advancements of uncooled infrared microbolometer materials: a review, *Sens. Actuators A Phys.* 342 (2022), 113611, <https://doi.org/10.1016/j.sna.2022.113611>.
- [25] D. Li, C.C. Menassa, V.R. Kamat, Non-intrusive interpretation of human thermal comfort through analysis of facial infrared thermography, *Energy Build.* 176 (2018) 246–261, <https://doi.org/10.1016/j.enbuild.2018.07.025>.
- [26] D. Li, C.C. Menassa, V.R. Kamat, Robust non-intrusive interpretation of occupant thermal comfort in built environments with low-cost networked thermal cameras, *Appl. Energy* 251 (2019), 113336, <https://doi.org/10.1016/j.apenergy.2019.113336>.
- [27] Y. He, H. Zhang, E. Arens, A. Merritt, C. Huizenga, R. Levinson, A. Wang, A. Ghahramani, A. Alvarez-Suarez, Smart detection of indoor occupant thermal state via infrared thermography, computer vision, and machine learning, *Build. Environ.* 228 (2023), 109811, <https://doi.org/10.1016/j.buildenv.2022.109811>.
- [28] A.C. Cosma, R. Simha, Thermal comfort modeling in transient conditions using real-time local body temperature extraction with a thermographic camera, *Build. Environ.* 143 (2018) 36–47, <https://doi.org/10.1016/j.enbuild.2018.06.052>.
- [29] Y. Wu, B. Cao, M. Hu, G. Lv, J. Meng, H. Zhang, Development of personal comfort model and its use in the control of air conditioner, *Energy Build.* 285 (2023), 112900, <https://doi.org/10.1016/j.enbuild.2023.112900>.
- [30] A. Aryal, B. Becerik-Gerber, A comparative study of predicting individual thermal sensation and satisfaction using wrist-worn temperature sensor, thermal camera and ambient temperature sensor, *Build. Environ.* 160 (2019), 106223, <https://doi.org/10.1016/j.buildenv.2019.106223>.
- [31] A. Ghahramani, G. Castro, B. Becerik-Gerber, X. Yu, Infrared thermography of human face for monitoring thermoregulation performance and estimating personal thermal comfort, *Build. Environ.* 109 (2016) 1–11, <https://doi.org/10.1016/j.buildenv.2016.09.005>.
- [32] X. Tian, R. Xu, W. Liu, Facial skin temperature and overall thermal sensation of sub-tropically acclimated Chinese subjects in summer, *J. Therm. Biol.* 112 (2023), 103422, <https://doi.org/10.1016/j.jtherbio.2022.103422>.
- [33] J.K. Choi, K. Miki, S. Sagawa, K. Shiraki, Evaluation of mean skin temperature formulas by infrared thermography, *Int. J. Biometeorol.* 41 (1997) 68–75, <https://doi.org/10.1007/s004840050056>.
- [34] D. Li, C.C. Menassa, V.R. Kamat, Non-intrusive interpretation of human thermal comfort through analysis of facial infrared thermography, *Energy Build.* 176 (2018) 246–261, <https://doi.org/10.1016/j.enbuild.2018.07.025>.
- [35] L. Lan, Z. Lian, W. Liu, Y. Liu, Investigation of gender difference in thermal comfort for Chinese people, *Eur. J. Appl. Physiol.* 102 (2008) 471–480, <https://doi.org/10.1007/s00421-007-0609-2>.
- [36] Q. Zhao, J. Lyu, H. Du, Z. Lian, Z. Zhao, Gender differences in thermal sensation and skin temperature sensitivity under local cooling, *J. Therm. Biol.* 111 (2023), 103401, <https://doi.org/10.1016/j.jtherbio.2022.103401>.
- [37] G.F. Volk, N. Wystub, M. Pohlmann, M. Finkensieper, H.J. Chalmers, O. Guntinas-Lichius, Quantitative ultrasonography of facial muscles, *Muscle Nerve* 47 (2013) 878–883, <https://doi.org/10.1002/mus.23693>.
- [38] H. Yoshikawa, A. Uchiyama, T. Higashino, ThermalWrist: smartphone thermal camera correction using a wristband sensor, *Sensors* 19 (2019), <https://doi.org/10.3390/s19183826>.
- [39] L. Lan, J. Tang, P. Wargozi, D.P. Wyon, Z. Lian, Cognitive performance was reduced by higher air temperature even when thermal comfort was maintained over the 24–28°C range, *Indoor Air* 32 (2022), e12916, <https://doi.org/10.1111/ina.12916>.
- [40] Y. Zhai, E. Arens, K. Elsworth, H. Zhang, Selecting air speeds for cooling at sedentary and non-sedentary office activity levels, *Build. Environ.* 122 (2017) 247–257, <https://doi.org/10.1016/j.enbuild.2017.06.027>.
- [41] Y. Zhai, Y. Zhang, H. Zhang, W. Pasut, E. Arens, Q. Meng, Human comfort and perceived air quality in warm and humid environments with ceiling fans, *Build. Environ.* 90 (2015) 178–185, <https://doi.org/10.1016/j.buildenv.2015.04.003>.
- [42] J. Zhou, X. Zhang, J. Xie, J. Liu, Occupant's preferred indoor air speed in hot-humid climate and its influence on thermal comfort, *Build. Environ.* 229 (2023), 109933, <https://doi.org/10.1016/j.buildenv.2022.109933>.
- [43] D.C. Montgomery, in: *Design and Analysis of Experiments*, John Wiley & Sons, 2008. <http://books.google.de/books?id=kMMJAm5bD3AC>.
- [44] L. Lan, Z. Lian, Application of statistical power analysis – how to determine the right sample size in human health, comfort and productivity research, *Build. Environ.* 45 (2010) 1202–1213, <https://doi.org/10.1016/j.buildenv.2009.11.002>.

- [45] Obesity: preventing and managing the global epidemic. Report of a WHO consultation, World Health Organ. Tech. Rep. Ser. 894 (2000) i-xii, 1–253, <https://www.ncbi.nlm.nih.gov/pmc/articles/PMC11234459/>.
- [46] M. Vellei, G. Chinazzo, K.-M. Zitting, J. Hubbard, Human thermal perception and time of day: a review, *Temperature* 8 (2021) 320–341, <https://doi.org/10.1080/23328940.2021.1976004>.
- [47] C. Lugaressi, J. Tang, H. Nash, C. McClanahan, E. Ubweja, M. Hays, F. Zhang, C.-L. Chang, M.G. Yong, J. Lee, W.-T. Chang, W. Hua, M. Georg, M. Grundmann, *MediaPipe: A Framework for Building Perception Pipelines*, 2019, 08172. ArXiv. abs/1906.
- [48] J. Gao, M. Liu, S. Wu, G. Liu, X. Wu, Z. Tian, X. Li, Y. Lv, Occupant's thermal responses to asymmetric radiant thermal environment with warm wall and cool ceiling, Part A: overall thermal responses, *Energy Build.* 286 (2023), 112950, <https://doi.org/10.1016/j.enbuild.2023.112950>.
- [49] Y. Wu, Z. Zhang, H. Liu, B. Li, B. Chen, R. Kosonen, J. Jokisalo, Age differences in thermal comfort and physiological responses in thermal environments with temperature ramp, *Build. Environ.* 228 (2023), 109887, <https://doi.org/10.1016/j.buildenv.2022.109887>.
- [50] B. Zhou, B. Jiao, B. Chen, C. Sun, L. Ding, Y. Ao, Physiological and perceptual responses of exposure to different thermal environments at low pressure (61.6 kPa), *Build. Environ.* 226 (2022), 109774, <https://doi.org/10.1016/j.buildenv.2022.109774>.
- [51] X. Yao, J. Crook, G. Andreeva, Enhancing two-stage modelling methodology for loss given default with support vector machines, *Eur. J. Oper. Res.* 263 (2017) 679–689, <https://doi.org/10.1016/j.ejor.2017.05.017>.
- [52] M. Papouskova, P. Hajek, Two-stage consumer credit risk modelling using heterogeneous ensemble learning, *Decis. Support Syst.* 118 (2019) 33–45, <https://doi.org/10.1016/j.dss.2019.01.002>.
- [53] F. Pedregosa, G. Varoquaux, A. Gramfort, V. Michel, B. Thirion, O. Grisel, M. Blondel, P. Prettenhofer, R. Weiss, V. Dubourg, J. Vanderplas, A. Passos, D. Cournapeau, M. Brucher, M. Perrot, É. Duchesnay, Scikit-learn: machine learning in Python, *J. Mach. Learn. Res.* 12 (2011) 2825–2830.
- [54] M. Luo, J. Xie, Y. Yan, Z. Ke, P. Yu, Z. Wang, J. Zhang, Comparing machine learning algorithms in predicting thermal sensation using ASHRAE Comfort Database II, *Energy Build.* 210 (2020), 109776, <https://doi.org/10.1016/j.enbuild.2020.109776>.
- [55] W. Zhang, Y. Wu, J.K. Calautit, A review on occupancy prediction through machine learning for enhancing energy efficiency, air quality and thermal comfort in the built environment, *Renew. Sustain. Energy Rev.* 167 (2022), 112704, <https://doi.org/10.1016/j.rser.2022.112704>.
- [56] Z. Qavidel Fard, Z.S. Zomorodian, S.S. Korsavi, Application of machine learning in thermal comfort studies: a review of methods, performance and challenges, *Energy Build.* 256 (2022), 111771, <https://doi.org/10.1016/j.enbuild.2021.111771>.
- [57] R.E. Wright, *Logistic regression*, in: *Reading and Understanding Multivariate Statistics*, American Psychological Association, Washington, DC, US, 1995, pp. 217–244.
- [58] W.S. Noble, What is a support vector machine? *Nat. Biotechnol.* 24 (2006) 1565–1567, <https://doi.org/10.1038/nbt1206-1565>.
- [59] A.H. Jahromi, M. Taheri, A non-parametric mixture of Gaussian naive Bayes classifiers based on local independent features, in: Artificial Intelligence and Signal Processing Conference, AISIP, 2017, pp. 209–212, <https://doi.org/10.1109/AISIP.2017.8324083>, 2017.
- [60] Wes McKinney, Pandas: a foundational Python library for data analysis and statistics. <https://pandas.pydata.org>, 2020. (Accessed 18 April 2023).
- [61] S. Khalid, T. Khalil, S. Nasreen, A survey of feature selection and feature extraction techniques in machine learning, in: Science and Information Conference, 2014, pp. 372–378, <https://doi.org/10.1109/SAC.2014.6918213>, 2014.
- [62] X. Tian, J. Yu, W. Liu, Facial skin temperature and its relationship with overall thermal sensation during winter in Changsha, China, *Indoor Air* 32 (2022), e13138, <https://doi.org/10.1111/ina.13138>.
- [63] T. Chaudhuri, D. Zhai, Y.C. Soh, H. Li, L. Xie, Random forest based thermal comfort prediction from gender-specific physiological parameters using wearable sensing technology, *Energy Build.* 166 (2018) 391–406, <https://doi.org/10.1016/j.enbuild.2018.02.035>.
- [64] J.-H. Choi, D. Yeom, Development of the data-driven thermal satisfaction prediction model as a function of human physiological responses in a built environment, *Build. Environ.* 150 (2019) 206–218, <https://doi.org/10.1016/j.buildenv.2019.01.007>.
- [65] L. Yang, S. Zhao, S. Gao, H. Zhang, E. Arens, Y. Zhai, Gender differences in metabolic rates and thermal comfort in sedentary young males and females at various temperatures, *Energy Build.* 251 (2021), 111360, <https://doi.org/10.1016/j.enbuild.2021.111360>.
- [66] J.-H. Choi, D. Yeom, Study of data-driven thermal sensation prediction model as a function of local body skin temperatures in a built environment, *Build. Environ.* 121 (2017) 130–147, <https://doi.org/10.1016/j.buildenv.2017.05.004>.
- [67] H. Pallubinsky, L. Schellen, T.A. Rieswijk, C.M.G.A.M. Breukel, B.R.M. Kingma, W. Van Marken Lichtenbelt, Local cooling in a warm environment, *Energy Build.* 113 (2016) 15–22, <https://doi.org/10.1016/j.enbuild.2015.12.016>.
- [68] Z. Wang, R. de Dear, M. Luo, B. Lin, Y. He, A. Ghahramani, Y. Zhu, Individual difference in thermal comfort: a literature review, *Build. Environ.* 138 (2018) 181–193, <https://doi.org/10.1016/j.buildenv.2018.04.040>.
- [69] W. Ji, R. de Dear, J. Kim, Y. Zhu, B. Cao, S. Liu, Study on the influence of climatic thermal exposure environment changed from cold to hot on human thermal preference, *Build. Environ.* 207 (2022), 108430, <https://doi.org/10.1016/j.buildenv.2021.108430>.
- [70] R.F. Rupp, J. Kim, R. de Dear, E. Ghisi, Associations of occupant demographics, thermal history and obesity variables with their thermal comfort in air-conditioned and mixed-mode ventilation office buildings, *Build. Environ.* 135 (2018) 1–9, <https://doi.org/10.1016/j.buildenv.2018.02.049>.
- [71] Z. Wang, H. Yu, M. Luo, Z. Wang, H. Zhang, Y. Jiao, Predicting older people's thermal sensation in building environment through a machine learning approach: modelling, interpretation, and application, *Build. Environ.* 161 (2019), 106231, <https://doi.org/10.1016/j.buildenv.2019.106231>.
- [72] J. Xiong, T. Ma, Z. Lian, R. de Dear, Perceptual and physiological responses of elderly subjects to moderate temperatures, *Build. Environ.* 156 (2019) 117–122, <https://doi.org/10.1016/j.buildenv.2019.04.012>.